Nanoscale iron (Fe_3O_4) surface charge controls Fusarium suppression and nutrient accumulation in tomato (*Solanum lycopersicum* L.)

Chaoyi Deng[1,2#], Yinhan Wang[2#], Christopher Castillo[3], Yinong Zhao[2], Wandi Xu[2], Jiapan Lian[4], Kevin Rodriguez-Otero[5], Hannah J. Brown[6], Keni Cota-Ruiz[7], Wade H. Elmer[8], Christian O. Dimkpa[1], Juan Pablo Giraldo[3], Yi Wang[1], Rigoberto Hernandez[2]*, Jason C. White[1]*

[1]Department of Analytical Chemistry, The Connecticut Agricultural Experiment Station, New Haven, Connecticut 06511, United States

[2]Department of Chemistry, Johns Hopkins University, Baltimore, Maryland 21218, United States

[3]Department of Botany and Plant Sciences, University of California, Riverside, Riverside, CA 92521, United States

[4]Ministry of Education (MOE) Key Laboratory of Environmental Remediation and Ecosystem Health, College of Environmental and Resources Sciences, Zhejiang University, Hangzhou 310058, China

[5]University of Puerto Rico-Cayey, Cayey, 00736, Puerto Rico

[6]Agronomy Department, University of Florida, Gainesville, FL 32603, United States

[7]Department of Biology, Utica University, Utica, New York 13502, United States

[8]Department of Plant Pathology and Ecology, The Connecticut Agricultural Experiment Station, New Haven, Connecticut 06504, United States

*Corresponding author.

E-mail address: r.hernandez@jhu.edu and Jason.white@ct.gov.

[#] Chaoyi Deng, and Yinhan Wang contributed equally.

Abstract

With the growing recognition that conventional agriculture will be unable to meet food production demands, innovative strategies to reach food security are imperative. Although nanoscale fertilizers are attracting increased attention as a sustainable platform for agricultural applications, limited data exists on how surface charge influences overall efficacy relative to disease suppression and nutrient accumulation. This study investigated the effect of positively and negatively charged iron oxide nanoparticles (Fe_3O_4 NPs) on the growth of tomato (*Solanum lycopersicum* L.) plants and their disease resistance against the pathogen *Fusarium oxysporum* f. sp. *lycopersici*at both the greenhouse and field scale. In addition, a theoretical model of the bio-interface was employed for mechanistic understanding of the interaction and attachment efficiency between NPs and tomato leaves after foliar exposure. In the greenhouse, both positively and negatively charged Fe_3O_4 NPs significantly suppressed Fusarium wilt by 41.4% and 44.6%, and increased plant shoot biomass by 327.6% and 455.0%, respectively, compared to the diseased control. The impact of NP surface charge was apparent; positively charged Fe_3O_4 NPs demonstrated superior efficacy compared to their negatively charged counterparts in mitigating disease damage and regulating nutrient (Na, Si, and Cu) accumulation. Computationally, positively charged Fe_3O_4 NPs consistently migrate toward lipid layers, indicative of a pronounced affinity between these entities compared to the negatively charged particles, which aligns with the experimental data. The findings highlight the importance and tunability of nanomaterials properties, especially the surface charge, in optimizing the use for disease suppression and nutrient modulation, which offers a great potential for sustainable agriculture.

Keywords: Nanoscale fertilizers, Iron oxide nanoparticles, Surface charge effects, Disease suppression, Fusarium, Nutrient biofortification, Computational modeling

TOC graphic

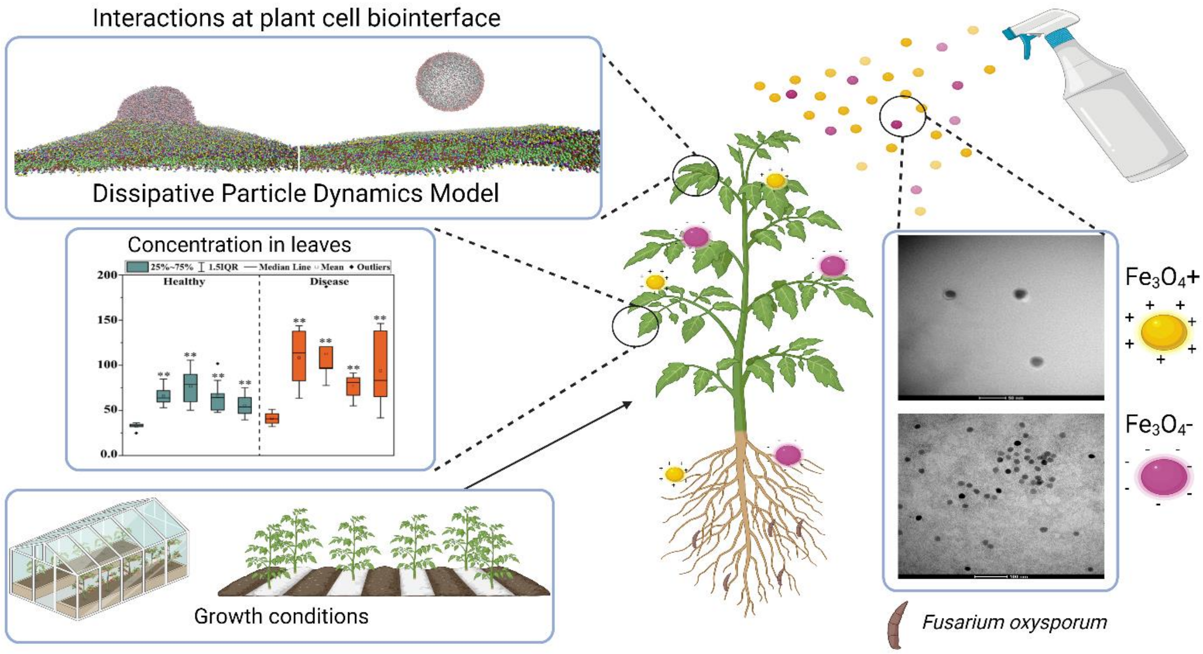

The graphic illustrates the impact of positively and negatively charged iron oxide nanoparticles (Fe_3O_4 NPs) on tomato growth and disease resistance, highlighting their potential as sustainable nano-enabled amendments.

1. Introduction

There is an urgent need for innovative agricultural strategies to enhance crop yields and meet the food demand of our rapidly growing population. In fact, it is estimated that food production will need to increase by 35% to 56% between 2010 and 2050. Meanwhile, the population at risk of hunger is projected to fluctuate between a decrease of 91% and an increase of 8% during the same period.[1] However, conventional agricultural practices are currently highly inefficient in their delivery and use of water and agrochemicals, resulting in suboptimum yields and significant secondary damage to the environment. For example, the delivery and use efficiency of the most widely used fertilizers is approximately 5-10%.[2] To compensate for these losses, growers are forced to overapply agrochemicals, resulting in high costs and product accumulation in the environment. Furthermore, the exacerbating effects of climate change are compounding the challenges faced by agricultural systems worldwide.[3] Increasingly unpredictable and extreme weather events are further diminishing crop yields and necessitating cultivation under more marginal and stressful conditions. Addressing these multifaceted issues and sustainably feeding the world in the face of a rapidly changing climate will undoubtedly emerge as one of the most formidable challenges of this century.[4]

The detrimental effects of pathogens on crop growth and productivity continue to be an issue of great concern, with data suggesting that on average, nearly 20% of crops are lost to plant disease.[5] Soil-borne fungal pathogens are particularly problematic as management options are limited; *Fusarium oxysporum* f. sp. *lycopersici* is among the most damaging of this group of fungal pathogens. In addition to decreasing crop yields overall, pathogens can also compromise nutritional quality and food safety through the production of mycotoxins. Fusarium wilt affects a broad range crop such as tomatoes (*Solanum lycopersicum* L.); the pathogen can infect plant roots, subsequently obstructing water and nutrient uptake from the soil. The resulting symptoms of the disease include leaf yellowing and wilting, and in severe cases, compromised flower and fruit production, and in some cases, mortality.[6,7] Consequently, there is a significant need for the development of safe, sustainable, and effective strategies to manage this damaging group of pathogens.

There has been rapidly increasing interest in the use of nanotechnology in agriculture, with nanoparticles (NPs) of a range of elements emerging as promising tools to augment fertilizer utilization efficiency, plant health, and crop biofortification.[8] As noted above, conventional agrochemical treatment options are inadequate, highlighting the necessity for novel management strategies such as nanotechnology that overcome these limitations.[9] Importantly, nanoscale materials have demonstrated efficacy in the management of a number of plant diseases, including Fusarium wilt.[10] Moreover, a number of these strategies do not primarily target the pathogen but instead seek to uniquely activate enhanced pathways metabolic defense against the pathogen, with the end result being significantly reduced damage from the disease. For example, Elmer and White reported that foliar application of 1 mg/mL CuO nanoparticles led to a 34% increase in the fresh weight of tomatoes grown in Fusarium-infected soil as compared to infected controls.[11] Similarly, Wang et al. observed that foliar and soil treatments with stearic acid-coated nano sulfur (200 mg/L) significantly increased the yield of Fusarium-infected tomatoes by 107% and 192%, respectively, compared to diseased controls. Importantly, treatment with conventional sulfur did not yield any benefit.[12] Furthermore, Lopez-Lima et al. found that the application of 1 mg/mL Cu-NPs notably reduced the symptoms of Fusarium wilt in tomatoes, decreasing both the incidence and severity by 68% and 66.5%, respectively, compared with controls. Additionally, the authors observed a significant promotion in tomato health, particularly evident in chlorophyll content, which increased from 19.3% to 28.6%.[13] The innovative application of sustainable and biocompatible nanomaterials may not only reduce pathogen-induced losses by enhancing plant immune system activity, but also can fortify the nutritional value of crops by enhanced mineral uptake.[14,15]

A number of previous studies have demonstrated the importance of nanomaterial properties such as morphology, dissolution profile, and charge to particle behavior and performance.[16] For example, Borgatta et al. demonstrated that foliar application of 10 mg/L $Cu_3(PO_4)$ nanosheets significantly suppressed fungal disease and increased biomass, but that for amorphous CuO NPs, concentrations above 100 mg/L were needed for an equivalent level of benefit.[17] Similarly, Ma et al. reported that foliar application of CuO nanosheets more effectively mitigated the detrimental effects of fungal infection on soybean biomass and photosynthesis that did other forms of nanoscale copper.[18] Deng et al. investigated the foliar application of nanoscale copper oxide (nanospike) with opposite surface charges to seedlings of field-grown tomato and watermelon that were infected with *Fusarium* pathogens. NP treatments not only significantly suppressed pathogen proliferation, but also increased yield and improved fruit nutritional content. Importantly, negatively charged materials significantly increased fruit Fe content (20-28%) over the positively charged particles, and the nanospike morphology exhibited superior performance over nanosheets as determined by a number of endpoints.[15] In addition, iron-based NPs have been recognized for their broad potential applicability in agriculture, such as facilitating nutrient transport,[19] enhancing seed germination and growth,[15] and enhancing disease management.[20] For example, seeds treated with 500 mg/L Fe_3O_4 NPs exhibited enhanced photosynthesis and leaf growth, as well as increased Fe and P content in leaves (20-27%) compared with controls.[21] Additionally, γ-Fe_2O_3 NPs have been reported to enhance chlorophyll levels (39.4%) in muskmelon, leading to greater growth (11.5%) and increased vitamin C content (46.95%) in the fruit compared with controls.[22] From this selection of the literature, it is clear that nanomaterial properties can dramatically impact overall beneficial impacts on plants, both under healthy and diseased conditions. Importantly, the specific role of surface charge of Fe-based NPs in suppressing *Fusarium* pathogens in crop species is poorly understood. Previous studies have shown that iron oxide NPs can promote plant growth and enhance plant disease resistance. Our work seeks to investigate the surface charge dependent effects of iron oxide NPs on plants subjected to different growth conditions.

Tomato was selected as the species for this work; this widely cultivated crop has significant nutritional value and considerable economic benefit. In the current study, nanoscale Fe_3O_4 (nFe_3O_4) with different surface charges was investigated for effectiveness against a *Fusarium* pathogen in tomato, as well as on crop nutritional content. Positively or negatively charged nFe_3O_4 were foliar applied to tomatoes that were subsequently cultivated under greenhouse and field conditions with or without infection by the fungal pathogen *Fusarium oxysporum f. sp. lycopersici*. Following a full life cycle investigation, mature fruits were harvested and agronomic parameters, Fe uptake, and nutrient content were evaluated. To increase understanding of the mechanisms of NP uptake and transport as a function of particle surface charge and pH, the interaction between the phospholipid bilayer and nFe_3O_4 was modeled using dissipative particle dynamics (DPD). This work increases our understanding of the use of nanoscale micronutrients to promote crop health and nutrient biofortification under healthy and diseased conditions, and advances efforts to develop sustainable nano-enabled strategies to increase agricultural output and decrease food insecurity in a changing climate.

2. Materials and Methods

2.1. Nanoparticle characterization and application

Negatively charged nFe_3O_4 was purchased from Ocean NanoTech (San Diego, California, USA), and positively charged nFe_3O_4 was synthesized through the modification of the negatively charged nFe_3O_4 using polyethylenimine (PEI) according to Kim et al.[23] PEI was chosen for its ability to bind with nanoparticles, enhancing their adhesion to plant surfaces and providing a stable positive surface charge. Bulk Fe and Ferric EDTA were obtained from Sigma-Aldrich (St. Louis, Missouri, USA). All nanoparticles were subsequently characterized for surface charge and hydrodynamic size using a Malvern Zetasizer Pro (Malvern Panalytical Inc, Massachussetts, USA). The instrument refractive index setting was 2.360 and the absorption setting was 0.147. The hydrodynamic sizes of the nanoparticles were measured at 12.5 nM in TES buffer (10 mM, pH 7.0). Similarly, the surface charge of nanoparticles was measured at a 12.5 nM in TES buffer (10 mM, pH 7.0) amended with 0.1 mM NaCl following previous methods.[24] The attenuated total reflection (ATR) of the nanoparticles was obtained using a Thermo Scientific Nicolet 6700 (Thermo Fisher Scientific, Massachussetts, USA). Transmission electron microscopy (TEM) images were obtained using Thermo Scientific™ Talos L120C™ TEM (Thermo Fisher Scientific, Massachussetts, USA). To prepare the TEM grid, NP suspensions of SHP- or SHP+ were made at 0.1 mg/mL in DI, briefly vortexed, and carefully dropped onto the Cu-based TEM grid (TED Pella, Inc.). Finally, Fiji software was used to obtain the size.

Select nanoparticle concentrations were determined by measuring absorbance from 450 to 850 nm using a UV-2600 Shimadzu spectrophotometer equipped with micro quartz cuvettes (10 mm x 2 mm, path length set to 10 mm; Kyoto, Japan) and by using the following equations[25]:

$$[Fe\ \frac{mg}{mL}] = \frac{(OD_{500} - OD_{800}) \times dilution\ factor}{5}$$

$$110 * [Fe\ \frac{mg}{mL}] = nM\ nanoparticle\ concentration \quad (1)$$

To prepare for greenhouse and field experiments involving foliar application of nFe_3O_4, the particles were mixed in 18MΩ Millipore water (MW) at a final Fe concentration of 250 mg/L. This concentration was chosen based on previous studies.[26,27] All treatments suspensions/solutions were freshly made and subjected to 25 min of sonication in a water bath (FS220 Ultrasonic Cleaner, Fisher Scientific) prior to use. There were five treatments in both *Fusarium*-infected (diseased) and *Fusarium*-non-infested (healthy) groups, including (1) Control; (2) Carboxyl coated Fe_3O_4 (SHP-); (3) Polyethylenimine coated Fe_3O_4 (SHP+); (4) Bulk Fe_3O_4 (Bulk Fe); (5) Ferric EDTA solution (Ionic Fe). The concentrations of Bulk Fe and Ferric EDTA were adjusted to match the molar quantity of Fe used in the nanoscale treatments.

In greenhouse and field experiments, each treatment had 10 and 9 replicates, respectively. The SHP- and SHP+ treatments were used to investigate the impact of particle surface charge on the biological response of both the plant and the pathogen. Bulk Fe was employed to discern effects attributed to size, while use of ionic Fe aimed to distinguish the effects of nanoscale materials from conventional ionic iron. Following sonication, leaves of twenty-one-day-old tomato seedlings were dipped into solutions of different Fe compounds for 1 min.[28] Control plants were treated with MW. The treated plants were subsequently transplanted for greenhouse or field studies.

2.2. Plant experiment design

Tomato variety Bonnie Best (*Solanum Lycopersicum* L.; Harris Seed Co., Rochester, NY) was chosen due to its widespread popularity and for its susceptibility to Fusarium pathogen infection as noted above.[12,15,29]

Seeds were germinated in plastic liners (72-cell, 5.66 X 5.66 X 4.93 cm^3) using potting soil substrate (Pro-Mix BX, Premier Hort Tech, Quakertown, Pennsylvania, USA) for three weeks before transplanting. No additional fertilizer was used during this period. Uniformly growing three-week-old seedlings were carefully selected for both greenhouse and field studies. The greenhouse study commenced in the Spring of 2022, while the field study took place during the Summer 2022. To prepare the pathogen inoculum, millet seeds (*Echinochloa esculenta*) were autoclaved in distilled water (1:1, wt:wt) for 1 hour and then seeded with agar plugs colonized with *Fusarium oxysporum* f. sp. *lycopersici* (FOL). After a 3-week incubation period at 22–25 ◦C, the millet was air-dried, ground, and sieved to a 1 mm consistency.[11] Prior to transplanting, 0.75 g of the prepared millet inoculum was hand-mixed into the planting holes prior to seedling addition.

In the greenhouse study, plastic pots (12.5 cm in diameter and 10 cm in height) were utilized after being cleaned with Millipore water (MW). The pots were filled with 0.5 L of potting soil. Throughout plant growth, the greenhouse temperature was maintained at a range of 25 ± 5 °C. Soil moisture was maintained at approximately 60% of field capacity through regular daily watering. No fertilizers were provided to the plants. For the field study, an experiment was set up at Lockwood Farm, which is part of the Connecticut Agricultural Experiment Station in Hamden, Connecticut. The microplots, set up with rows 0.9 m wide and 6 m apart, received 112 kg/ha of 10-10-10 NPK fertilizer prior to planting. Plots were covered with black plastic mulch and irrigated as needed through drip tape. Thirty microplots were created within each row, spaced 30 cm apart. For both the greenhouse and field trials, seedlings treated with experimental materials were transplanted in a randomized block design.

Throughout the study, we assessed plant disease progression weekly by evaluating the shoot system phenotype. Using the area-under-the-disease-progress-curve (AUDPC) method of Jeger et al., a scale ranging from 1 to 5 was used to determine disease severity: 1 represented healthy plants, while 5 signified those plants that were completely stunted or deceased, enabling accurate evaluation of the extent of disease impact.[30] To quantify disease progression, we computed the AUDPC using the trapezoid rule.

$$\text{AUDPC}(\tfrac{1}{2}[t_{(i+1)} + t_i]) = \tfrac{1}{2}\,(D_i + D_{(i+1)}) \times (t_{(i+1)} - t_i) \quad (2)$$

where D_i is the disease rating at time t_i.

2.3. Plant harvest and elemental analysis

After a 90-day growth period, the tomato plants were harvested. In the greenhouse study, shoot and root biomass was determined. For the field study, both shoot and fruit biomass were measured. Subsequently, root, shoot and fruit samples were cleaned with DI water to eliminate any surface-adhering particles and then placed in pre-labeled paper bags for oven drying at 70°C for 72 hours. Approximately 0.2 g of the dried sample was weighed into digestion tubes amended with 3 mL of plasma-pure nitric acid (HNO_3; Fisher Scientific, Massachussetts, USA). The samples were digested at 115°C for 45 minutes using a hot block (DigiPREP MS, SCP SCIENCE, Quebec City, Canada). The digests were diluted to 50 mL using DI water. For elemental analysis, the digests of three replicate samples of each tissue were analyzed by inductively coupled plasma optical emission spectroscopy (ICP-OES)(iCAP 6500, Thermo Fisher Scientific, Massachussetts, USA) to determine both macro- (Ca, K, Mg, Na) and micro (Si, Fe, Mn, Cu) nutrient levels. As part of the QA/QC protocol, blanks (no plant tissues), Fe spikes (1, 5, 10, 50 mg Fe/kg Fe_2O_3 powder), and standard reference materials (NIST-SRF 1570a and 1547, New Jersey, USA) were included. Yttrium (Y) served as an internal standard, with a continuing calibration verification (CCV) sample (1 ppm Fe) analyzed every 20 samples to ensure precision. The recovery rate for all analyzed elements was 85-115%.

2.4. Computational analysis

Given the importance of nanomaterial interactions at the plant cell biointerface, we used computational methods to investigate the binding affinity of Fe_3O_4 NPs to the cell membrane under three different pHs regimes: 6, 7 and 8. All simulations are carried out by Large-scale Atomic/Molecular Massively Parallel Simulator (LAMMPS),[31] and dissipative particle dynamics (DPD) were used to model the binding between lipid bilayer and NPs.

The DPD force field are described by the now-standard equations[32]:

$$F_i = \sum_{j \neq i} \left(F_{ij}^C + F_{ij}^D + F_{ij}^R \right), \tag{3}$$

where

$$F_{ij}^C = \begin{cases} a_{ij} w\left(r_{ij}\right) \widehat{r_{ij}}, & r_{ij} < R_c \\ 0, & r_{ij} \geq R_c \end{cases} \tag{4}$$

$$F_{ij}^D = -\gamma w^2\left(r_{ij}\right)\left(\widehat{r_{ij}} \cdot \overrightarrow{v_{ij}}\right)\widehat{r_{ij}} \tag{5}$$

$$F_{ij}^R = \sigma w\left(r_{ij}\right) \theta_{ij} \widehat{r_{ij}} \tag{6}$$

and

$$w\left(r_{ij}\right) = 1 - \frac{r_{ij}}{R_c} \tag{7}$$

where $w\left(r_{ij}\right)$ is a weight function, R_c is the cutoff value for the DPD model, F_{ij}^C is the constant force term, F_{ij}^D is the dissipative force term, and F_{ij}^R is the random force term.[33] The dissipative force F_{ij}^D and the random force F_{ij}^R are correlated through the fluctuation-dissipation theorem:

$$\sigma^2 = 2\gamma k_B T \tag{8}$$

The Coulomb interaction is also involved in the DPD system with a correction to the charge density[34]:

$$\rho(r) = \frac{q\beta^2}{\pi r} \exp(-2\beta r) \tag{9}$$

where β is the so-called softening parameter imposing a decay in the long-range interaction.

The resulting softened Slater potentials and forces are[34]:

$$U_{ij} = \frac{\Gamma q_i q_j}{4\pi r_{ij}} \left[1 - \left(1 + \beta r_{ij}\right) \exp(-2\beta r_{ij})\right] \tag{10}$$

$$\overrightarrow{F_{ij}}^E = \frac{\Gamma q_i q_j}{4\pi r_{ij}} \left[1 - \exp\left(-2\beta r_{ij}\right) \left(1 + 2\beta r_{ij}\left(1 + \beta r_{ij}\right)\right)\right] \frac{\overrightarrow{r_{ij}}}{r_{ij}} \tag{11}$$

The softened potential is illustrated in Fig S2.

In previous work, we constructed a DPD model that can be transformed from the MARTINI model, while conserving most of the parameters in the MARTINI force field.[33] During this process, key molecular characteristics such as the radius of gyration and the root mean square of sample proteins are preserved. Here, we employ this coarse-grained representation to simulate the interaction between the nanoparticle and membrane lipids. The nanoparticle models are built as a spherical, rigid FCC (Face-centered cubic) lattice, formed by DPD particles parametrized from C5 MARTINI particles.[35] Water molecules in the simulation are further coarse-grained into beads containing 20 water molecules. They are coarser than typical MARTINI model beads with 4 water molecules each. For a large system such as the one addressed in this work, the use of a grosser coarse-graining significantly reduces the computational cost, while retaining most of the properties we are interested in—namely, the interactions between nanoparticles and lipids—as described below.

The cell membrane is simulated as a lipid bilayer with a large number of distinct lipid molecules with specified compositions. Specifically, the lipid composition was adopted from published experimental data of Popko[36] as reproduced here in Table S1. Lipid bilayers were generated using the Charmm-GUI MARTINI bilayer maker.[37–39] We excluded diacylglycerol lipids, as they predominantly reside in plastids[36] and are not represented in the MARTINI model.

2.5. Statistical analysis

Agronomic and elemental content data were analyzed using the Statistical Package for the Social Sciences program 26 (SPSS 26, Chicago, IL, USA). Mean values of the control group and treatments were compared using a one-way ANOVA and Tukey-Kramer multiple comparison test. Additionally, a student's t-test was employed to compare differences between the control group and specific treatments. Outliers were identified using the 1.5 IQR method. The results are presented as mean ± standard error (SE), and statistical significance was determined at a threshold of $P < 0.05$ or $P < 0.01$.

3. Results and discussion

3.1. Nanoparticle characterization

TEM images of the two Fe based nanomaterials (SHP- with -COOH and SHP+ with PEI modification on the surfaces) are shown in Figure 1. Both particles exhibit a spherical shape; the average size of SHP- and SHP+ are 21.00 ± 2.97 nm, and 20.8 ± 2.76 nm, respectively. Figure 2 shows their ATR spectrum, revealing a Fe-O peak around 570-590 cm^{-1} for both particles, indicating the presence of iron oxide. SHP- NPs exhibit peaks at 3250 (OH stretch), 1650 (C=O stretch), and 1050 (C-O stretch) cm^{-1} (Figure 2A); for SHP+ NPs, significant peaks are at 3420 (NH stretch), 2900 (C-H stretch/N-H stretch), 1620 (N-H bending), 1470 (C-H bending), and 1040 (C-N stretch) cm^{-1} (Figure 2B). These findings align with previous reports,[40,41] confirming the successful coating of the NPs. Moreover, Dynamic Light Scattering (DLS) measurements (Figure S1) confirmed that the SHP+ possess a positive ζ potential of 37.43 ± 1.52 mV and hydrodynamic size of 47.9 ± 32.5 nm, while the SHP- possess a negative ζ potential of -24.52 ± 1.89 mV and hydrodynamic size of 35.5 ± 17.0 nm.

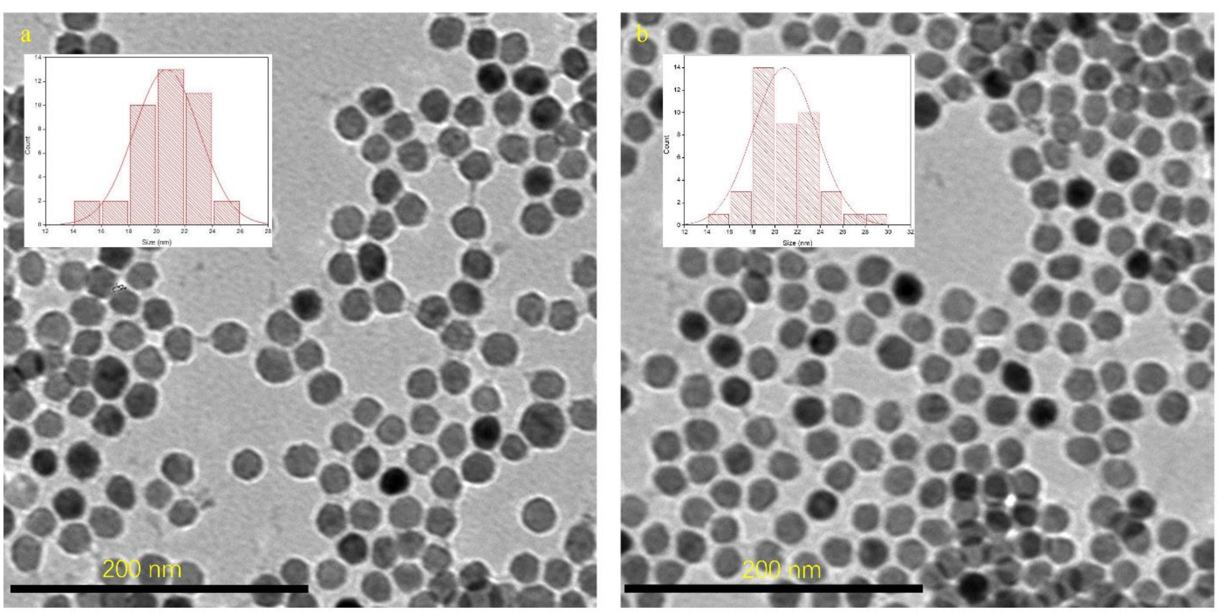

Figure 1. Representative TEM micrographs of a. negatively charged nano Fe_3O_4 (SHP-), b. Positively charged nano Fe_3O_4 (SHP+). The scale bar is 200 nm.

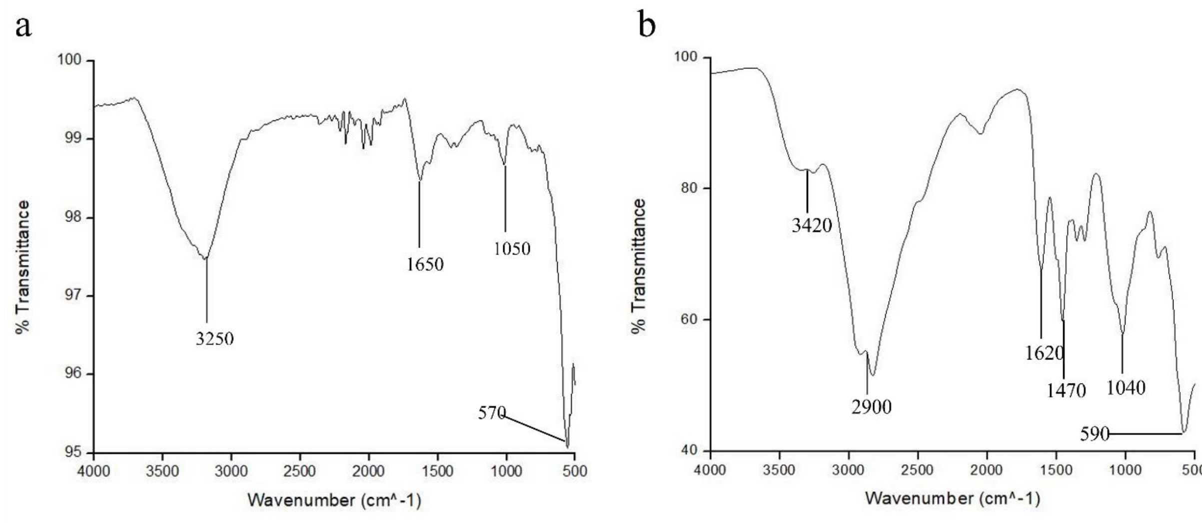

Figure 2. ATR spectrum of a. SHP-, and b. SHP+

3.2. Effect of NPs on plant growth and disease severity

Figure 3a and b show plants from the greenhouse trial, categorized into healthy and disease groups with different Fe-based treatments. Apparent visual differences can be observed between *Fusarium* infected individuals and healthy controls, where infection inhibited plant shoot growth. The role of iron-based materials in suppressing disease was assessed using the AUDPC method. In the greenhouse (Figure 3e), all treatments showed a significant decrease in AUDPC compared to the diseased control. Notably, SHP- and SHP+ decreased AUDPC by 41.4% and 44.6%, respectively, compared to the diseased control; these values are statistically equivalent. The fresh shoot and root biomass are shown in Figure 3c. It is evident that fungal infection has a significant impact on the biomass of plants. Compared to the control group of healthy plants, the diseased controls exhibited a reduction of 86.3% and 68.5% in shoot and root biomass, respectively. In the healthy group, nanoscale treatments did not significantly impact plant shoot or root biomass compared to the control. However, bulk Fe decreased the shoot biomass by 21.5%, and ionic Fe decreased the shoot and root biomass by 18.1% and 33.3%, respectively. Interestingly, in the infected groups, all Fe-based treatments alleviated disease damage, increasing both shoot and root biomass compared to the disease control, with SHP+ showing the best performance. Specifically, SHP- and SHP+ increased shoot biomass by 327.6% and 455.0%, and increased root biomass by 190.1% and 192.1%, respectively, compared to the control. However, there was no significant difference between these nanoscale materials as a function of charge. Previous research has reported the beneficial effects of Fe based NPs; Zia-Ur-Rehman et al. found that soil applied Fe^0 NPs (25 mg/kg) increased the dry mass of wheat roots, shoots, and grains by 46%, 59%, and 77%, respectively, compared to the untreated controls.[42] Li et al. found that exposing roots to 50 mg L^{-1} of Fe_3O_4 NPs under hydroponic conditions improved rice growth under iron deficiency, also increasing chlorophyll content by 26.9%. In addition, the concentration of oxidative stress biomarkers and stress-related phytohormones in rice such as gibberellin and indole-3-acetic acid have been shown to be reduced by 50 mg L^{-1} of Fe_3O_4 NP treatment compared to the untreated control.[43]

In the field trial (Figure 3f), all treatments except the bulk Fe exhibited a significant decrease in AUDPC compared to the disease control. It is noteworthy that SHP+ demonstrated the most substantial decrease in AUDPC, reducing it by 42.7%, which is in line with the findings from the greenhouse study. Elbasuney et al. observed that colloidal ferric oxide nanoparticles not only promote plant growth but also suppress Fusarium wilt disease in tomato plants. Specifically, at 20 μg/mL, the particles reduced disease indices by 15.62% and offered substantial protection against the pathogen.[44] In the current study, *Fusarium* infection decreased tomato shoot and fruit biomass by 43.6% and 54.2% relative to the heathy plants, respectively (Figure 3d). Notably, in the healthy group across all treatments, only SHP+ significantly increased shoot biomass (by 68.3%) compared to the healthy control. However, SHP+ did not significantly increase shoot biomass in the infected plants, which is different from the greenhouse study. This difference is likely a function of the complexity encountered in field studies, where a range of environmental factors often impact results. However, noticeable trends are evident and are consistent with the greenhouse study. Similar findings were observed with yield; SHP+ non-significantly increased fruit yield in both healthy and disease groups by 24.7% and 19.6% compared to each control, respectively.

Overall, both SHP- and SHP+ improved tomato growth in the presence and absence of *Fusarium*, with more pronounced effects being observed under the more controlled greenhouse conditions. Although the field results were not statistically significant due to the high variability among the replicates, the trends do highlight the potential to enhance yield and bring economic benefits to farmers while minimizing agrochemical use. Previous research has shown that iron NPs (40 μM Fe_2O_3) have the potential to enhance the growth of grape (*Vitis vinifera* L.) plants under PEG-induced drought stress by modulating leaf antioxidants.[45] Additionally, the application of Fe_3O_4 nanoparticles at 20 mg/L has been shown to enhance both shoot and root growth of Red Sails lettuce (*Lactuca sativa* L.) in chromium-contaminated soil by 53% and 76% compared with control, respectively. This beneficial effect was attributed to the heightened activity of antioxidant enzymes.[46] Furthermore, surface modification holds greater potential within this domain. Lau et al. determined that seed treatment with polycaprolactone-coated Fe_3O_4 nanoparticles (positively charged) in tomato (*Solanum lycopersicum*) did not impede seed germination and that the functionalized nanoparticles possess the capability to serve as a versatile platform for delivering active compounds, including fungicides and growth factor agents.[47] Meanwhile, Iannone et al. reported that citric acid coated Fe_3O_4 nanoparticles (negatively charged) acted as stimulants for the growth of soybean (*Glycine max* L.) and alfalfa (*Medicago sativa* L.), increasing chlorophyll levels, enhancing plant development, and improving productivity.[48] These findings from the literature align with our current results. Nevertheless, it's notable that the variance in charge between Fe_3O_4 NPs had non-significant impact in our work, the exception being for the field-measured AUDPC.

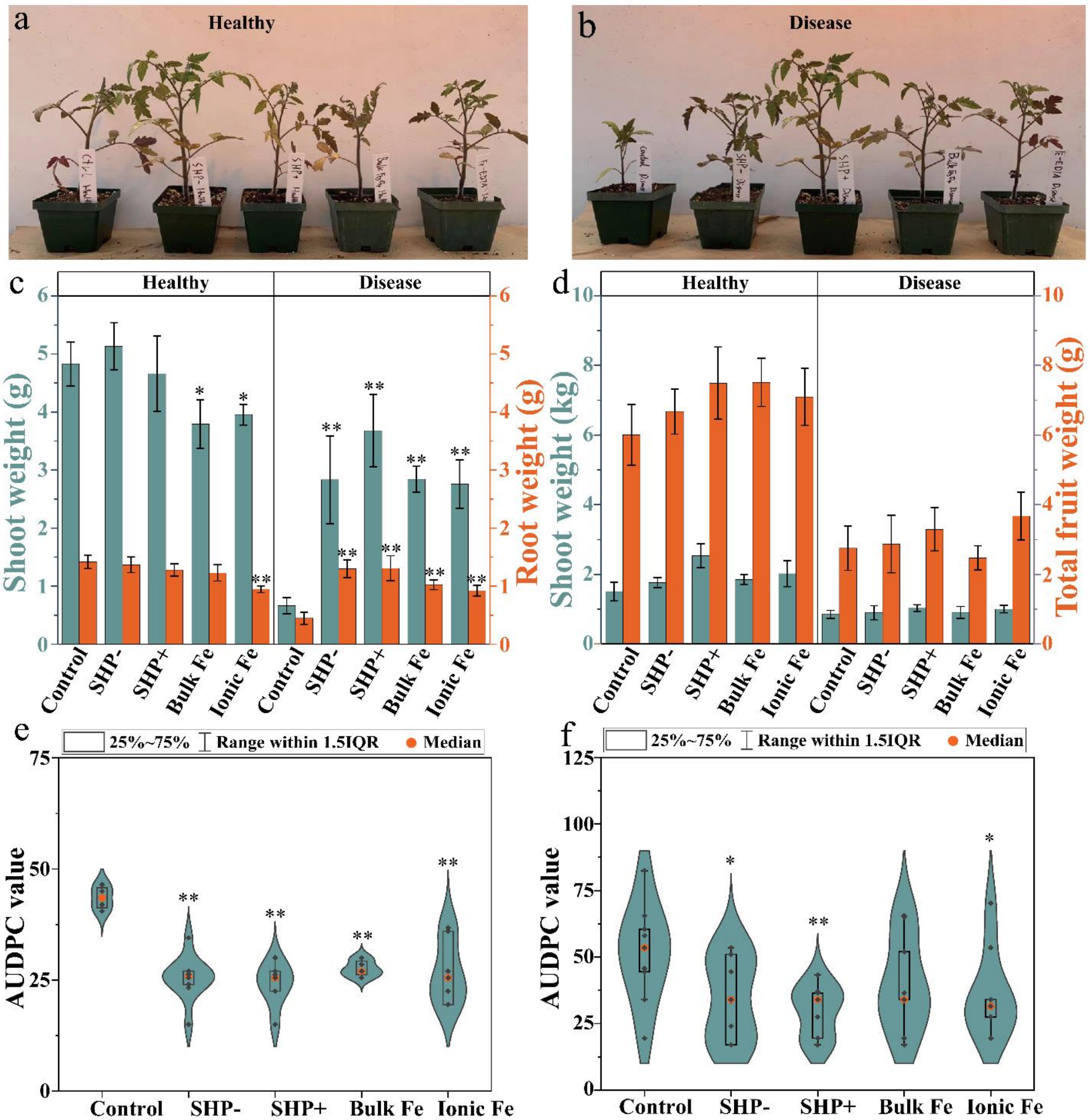

Figure 3. Physiological response of healthy and Fusarium-infected tomato seedlings upon foliar exposure to differently charged Fe NPs at 50 mg/kg Fe. (a) Phenotypic images of healthy tomato seedlings across different treatments. (b) Phenotypic images of Fusarium-infected tomato seedlings across different treatments. (c) Shoot weight and root weight of healthy and Fusarium-infected tomato seedlings in the

greenhouse experiment. (d) Shoot weight and total fruit weight of healthy and Fusarium-infected tomato in field experiment. AUDPC was measured using the Area-Under-Disease-Progress-Curve method for a Fusarium-infected tomato in a (e) greenhouse and (f) field experiment. Statistical significance between the control and Fe treatments at $p < 0.05$ and $p < 0.01$ is reported as labeled by * and ** respectively.

3.3. Fe content in tomato post-harvest

In the greenhouse, the shoot and root Fe content was measured (Figure 4). Under healthy conditions, SHP- and SHP+ significantly increased the shoot Fe content by 103.8% and 136.5% compared to the healthy controls, respectively (Figure 4a). A similar trend was observed in the diseased group, where both NPs treatments significantly increased Fe content compared to the untreated diseased control (by 164.8% and 175.3%, respectively). There was no significant difference between the nanoscale materials as a function of charge. Interestingly, all treatments generally reduced Fe accumulation in the roots (Figure 4b). Specifically, in the healthy group, except for ionic Fe, all treatments significantly decreased Fe concentration from 26.2-40.0% compared to the healthy control. It is noteworthy that while SHP+ significantly increased Fe concentration in the shoots to the greatest extent, it also caused the most substantial reduction in Fe concentration in the roots (by 40%). In the disease group, a similar pattern is evident, where all treatments, except for SHP-, significantly decreased Fe concentration in the roots from 33.3-40.4%, when compared to the diseased control. Specifically, SHP+ exhibited the most substantial reduction of 38.6%. These findings are likely attributed to the fact that all treatments were foliar applied, and minimal transfer to the roots occurred. Additionally, plants primarily acquire Fe through root uptake,[49] and when a substantial amount of Fe is obtained by foliar application, the mechanisms responsible for acquisition from soil may be significantly downregulated.

The observed disease suppression with Fe based treatments is likely a function of the elevated Fe content in the shoots. Iron is a critical micronutrient and plays a crucial role in chlorophyll formation, which is essential for photosynthesis. It also contributes to the catalytic capabilities of enzymes that are involved in plant defense metabolism, as well as in the regulation of plant growth and development.[50] Therefore, plants may benefit from the presence of abundant foliar supplied iron, which promotes overall health, aids in their growth, and leads to enhanced resistance to disease and increased crop yields under biotic stress. A number of recent studies have also demonstrated the potential of foliar nanoscale micronutrients to enhance tolerance to biotic and abiotic stressors. Notably, the enhanced disease tolerance is a function of modulated nutrition, with increased expression of defense and antioxidant-related genes. For example, Wang et al. reported on the mechanisms of disease suppression by sulfur NPs in tomato plants through an orthogonal investigation using two photon-microscopy, gene expression analysis, and time-dependent metabolomics, and found a nanoscale specific assimilation pathway of S NP that lead to the upregulation of genes related to disease resistance and biosynthesis of defensive metabolites.[29] In addition, the application of nanoscale micronutrients can promote plant development and health by enhancing the plant metabolic profile and important bio-synthetic pathways.[51,52] Importantly, tomato plants are known to be particularly susceptible to Fe deficiency, especially under conditions such as high soil pH or poor Fe availability. Dimkpa et al. found that the availability of iron in soil is constrained by the formation of insoluble ferric [Fe^{3+}] complexes, particularly evident in neutral to alkaline pH conditions. Consequently, at the pH levels common in many soils, the majority of iron becomes bound within the soil, making it predominantly inaccessible to soil microbes and plants.[53] To counter the resulting Fe deficiency in plants, supplementing Fe through fertilizers is a common practice. However, due to the challenges mentioned above (soil pH, low utilization rate), the efficacy of applying Fe fertilizer to soil is not always cost effective. Hence, foliar application of Fe fertilizers, particularly in nanoscale form, may be an important supplementary method, particularly in the presence of fungal pathogens in the soil. For example, Sharma et al. reported that foliar application of nano-Fe_2O_3 significantly increased both the iron content and yield of rice grain, highlighting the potential of this supplementation method to be an effective nano-enabled strategy to increase agronomic performance.[54]

3.4. Simulation of interactions between Fe NPs and the plant leaf as a function of charge

To provide mechanistic insight into the interaction between differentially charged NPs and plant tissues in the leaf, we analyzed the temporal progression of the distance between NPs and a lipid bilayer, as illustrated in Figure 5. Specifically, nFe_3O_4 NPs were modeled as hollow entities, significantly reducing the computational load compared to a solid counterpart. These structures are composed of C5 MARTINI beads arranged in a FCC lattice. The edge length of the lattice (L_{fcc}) was set to $\frac{4}{3}^{(1/3)}$ in reduced DPD units, representing an idealized crystal truncation. The mass of each NP constituent was determined by dividing the total NP mass by the number of particles, reflecting the hollow particle approximation. During simulations, NPs were treated as rigid bodies so as to focus solely on their interactions with lipid bilayers.

The charged interface between NPs and the bilayer was tailored by attaching the requisite functional groups to the surface of the NPs. Negatively charged NPs featured surface-tethered carboxylic acids represented by MARTINI Q_a beads. These were chemically bonded to the NP surface with a substantial bond constant (30,000 kJ/mol·nm^2) and a bond length of 0.4 nm. The bead distributions were randomized over the NP surface with a density derived from the charge densities reported by Murphy et al.[55] For the targeted pH environment, this density was consistently maintained. Conversely, positively charged NPs were modeled by affixing linear polyethyleneimine (PEI) as in the MARTINI model of Mahajan and Tang.[56] The PEI polymer, composed of P2 and Qd beads, was constructed according to the bond, angle, and dihedral parameters from the aforementioned model while disregarding unprovided parameters. To address the pH-sensitive charge state of PEI, several variants corresponding to different pH conditions were investigated. Each PEI chain consisted of 77 monomers, aligning with the molecular weight specified in the experiments. A total of 98 PEI chains were wrapped around each NP, resulting in approximately 3770 positive charges at pH 7, with appropriate adjustments made for pH 6 and pH 8 while keeping the polymer length and chain count constant. To access pH=6 and pH=8, the number of charged particles on PEI was varied following the method of Mahajan and Tang.[56]

In the simulations, we observed that positively charged NPs consistently migrate toward the lipid layers, indicative of a pronounced affinity between these entities. This behavior is in agreement with the enhanced

Fe content observed in plant shoots in the greenhouse experiments (Figure 4a). In addition, the final state in the simulations suggests the SHP+ has partially penetrated the lipid bilayer, indicating cell membrane permeability of the NP. Conversely, negatively charged NPs demonstrate an aversion and negligible binding to the bilayer as they remained apart by a significant distance throughout all the simulations with varied specified conditions. The binding affinity of SHP+ is also affected by the pH of the solution: binding was seen to be less likely at pH=6, as compared to pH=7 and pH=8. The computational findings regarding the effect of charge on NPs binging and uptake align with our experimental observations, where a notable increase in biomass was recorded following treatment with SHP+, as well as increased Fe shoot content in the healthy treatments. This phenomenon may be ascribed to the cellular membrane's preference for iron uptake, facilitated by the presence of positively charged moieties on the NPs surface, thereby enhancing cellular internalization. Meanwhile, variations in pH can influence the binding affinity of SHP+. Previous studies indicate that plant cells tend to be somewhat acidic.[57] Consequently, when SHP+ particles penetrate plant cells, they become trapped inside due to the reduced binding affinity with the cell membrane. Consequently, there appears to be a reduced vulnerability of the plants to the disease challenges presented, as evidenced by the simulation and empirical data. This underscores the critical role of surface charge in NPs-cell interactions and its potential impact on disease susceptibility in plants. Conversely, the higher Fe content in the SHP- treatment of the diseased plants may be due to leaf surface chemistry changes induced by fungal infection. The caveat to this hypothesis is that it has emerged from indirect evidence obtained from a simplified model of the NP plan interaction in tandem with the experimental observations of the actual system. More direct proof and deeper understanding of interactions inside leaf cells requires additional experimental and computational studies evaluating the iron transporter proteins under healthy and diseased growth conditions.

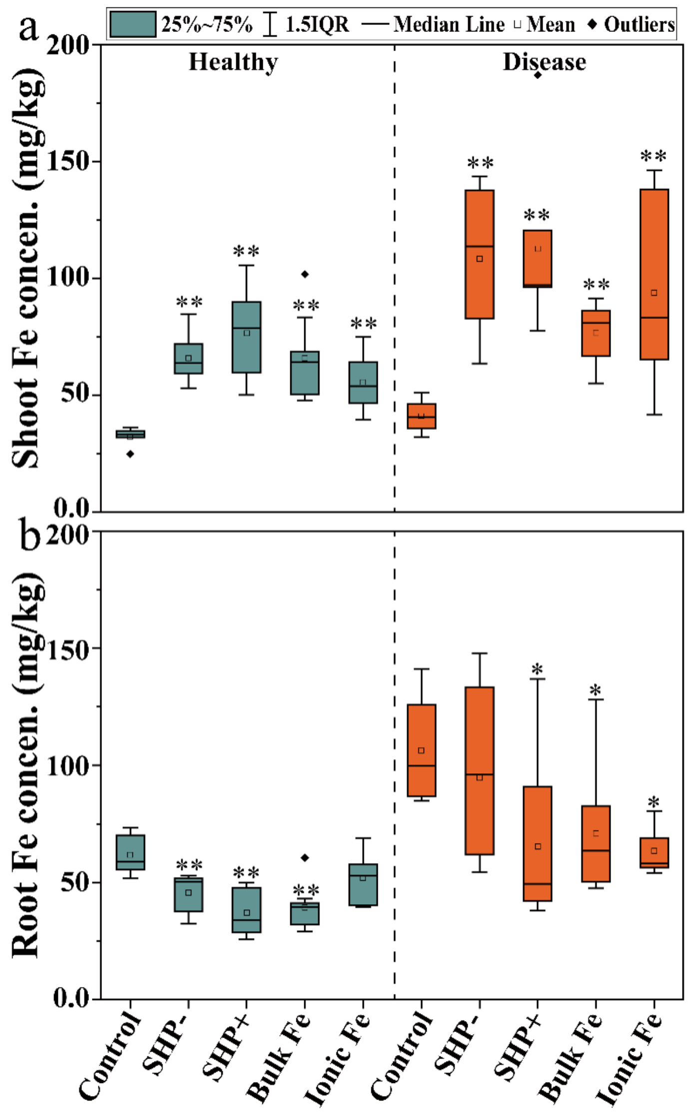

Figure 4. Fe concentration in greenhouse-grown tomato (a) shoot and (b) root tissues. Statistical significance between the control and Fe treatments at $p < 0.05$ and $p < 0.01$ is reported as labeled by * and ** respectively.

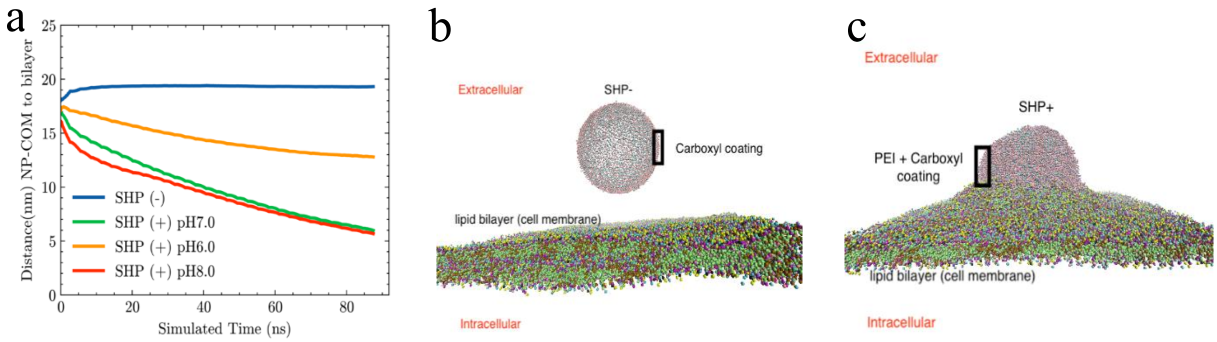

Figure 5. Two types of nanoparticles (SHP+ under three different pHs and SHP-) simulated for 90ns. (a) The distance of the center of mass of each type of nanoparticle to the surface of the lipid bilayer. SHP+ NP shows a trend to bind with lipid bilayer under different pH levels, while SHP- NP shows a trend to remain unbound with lipid bilayer. SHP+ binds more effectively at pH=7 and pH=8, compared to pH=6. (b) Final configuration of the simulated SHP- with lipid bilayer. The nanoparticle is unbound. (c) Final configuration of the simulated SHP+ with lipid bilayer. The nanoparticle is embedded, and has partially penetrated the lipid bilayer. The simulation suggests SHP+ nanoparticle has cell membrane permeability in plants.

3.5. Effect of surface charge on plant nutrient accumulation

The changes in plant macro- and micro-element uptake and translocation were determined as a function of disease presence and treatment (Figure 6 and Table S2). Nanoscale Fe treatments affected plant nutrient element accumulation as a function of charge. Interestingly, disease induced changes in the content of Na, Si, and Cu were observed, but SHP+ reverted those stress-induced changes in several instances. In addition, significant interaction was evident between SHP+ and the disease.

Fungal infection significantly increased the Na content (2806.8 mg/kg) in plant shoots by 230.6% compared to the healthy control (849.0 mg/kg); this finding is indicative of overall stress as a function of infection. SHP+ markedly alleviated this impact, reducing the shoot Na concentration by 21.3% and 52.2% in comparison with SHP- and the diseased control, respectively (Figure 6d). Although Na is not an essential nutrient for plants, it can significantly affect plant growth and physiology, and serves as an indicator of biotic and abiotic stresses. Excessive Na levels can induce phytotoxicity, including leaf chlorosis and necrosis, as well as an overall decline in plant health;[58] however, at lower concentrations, Na can promote metabolism, including photosynthesis. Different responses were observed in the healthy groups under the same treatment. For example, in healthy plant shoots, SHP+ increased the Na content by 24% and 32.3% compared to SHP- and the healthy control, respectively (Figure 6a). A significant interaction effect was again demonstrated between SHP+ and the disease, since SHP impacted Na content only under infection. This is consistent with the shoot biomass data presented above, where SHP+ did not promote plant growth in the absence of fungal infection, while in diseased plants, SHP+ counteracted the negative impact of the pathogen on growth. Under both healthy and diseased conditions, both SHP+ and SHP- increased shoot Fe accumulation to a similar extent (Figure 4a). Thus, Fe level may not be the only factor impacting plant response. More complex interactions can occur between SHP+, PEI, the plant, and the pathogen. Further mechanistic and molecular investigations are needed to understand these processes. For example, Wang et al. applied S NPs with different surface modifications to tomato plants[29] and reported significantly different phenotypic responses to different S NP types but with a similar level of S uptake in plant tissues. The authors used time-dependent gene expression and metabolomics analyses to demonstrate a distinct S NPs assimilation pathway that uniquely impacted plant response and health under disease pressure.[29]

Interestingly, disease significantly increased Si content in plant roots by 23.6% compared to the healthy control (135.5 mg/kg), although both nanoscale treatments reduced Si content in healthy tomato roots. Notably, SHP+ decreased root Si content by 30% compared to SHP-. Although disease did not alter Si shoot content, SHP+ increased shoot Si concentration in both healthy and diseased conditions by 24% and 32.5% compared to the SHP- treatment, respectively (Figure 6b, e). This surface charge-specific phenomenon may be attributed to the decreased competition between positively charged nanoparticles and silicon/silicic acid for uptake by plant roots as compared to negatively charged nanoparticles. Consequently, in the presence of positively charged nanoparticles, Si uptake may be less impeded, leading to elevated silicon content in plant shoots. Importantly, previous research suggests that silicon (Si) can have beneficial effects on plant growth, stress tolerance, and disease resistance, due to its potential to enhancing the structural integrity of plant cell walls, thereby fortifying them against the biotic and abiotic stresses.[59,60] Disease significantly increased Cu content in plant roots (17.0 mg/kg) by 47.3 % compared to the healthy control (11.6 mg/kg). SHP+ markedly alleviated this change (10.6 mg/kg) and reduced Cu concentration back to levels equivalent to the healthy control, reducing the Cu content by 34.3% and 37.6% compared to SHP- and the diseased control, respectively. Again, there is a clear charged based difference as SHP- did not alleviate the disease-induced changes in Cu content.

In summary, these results indicate that the surface charge of nanoparticles (SHP+ vs SHP-) significantly influences nutrient element absorption and distribution within plants under disease pressure, with SHP+ demonstrating superior performance compared to the SHP-. While we did not observe significant alterations in Fe content based on its charge, distinct differences in phenotype and the content of other nutrients/elements were evident based on charge characteristics. These findings of charge-based differences provide valuable information for the future design and optimization of nanofertilizers, although precise impacts may differ based on nanoparticle type and plant species. Further mechanistic investigations are necessary to understand in greater detail the time-dependent molecular basis of nanoscale interactions at the leaf biointerface as a function of charge and particle transformation; such understanding will then allow the optimization of nanoscale micronutrient fertilization strategies for nano-enabled agricultural efforts to increase food production and decrease food insecurity.

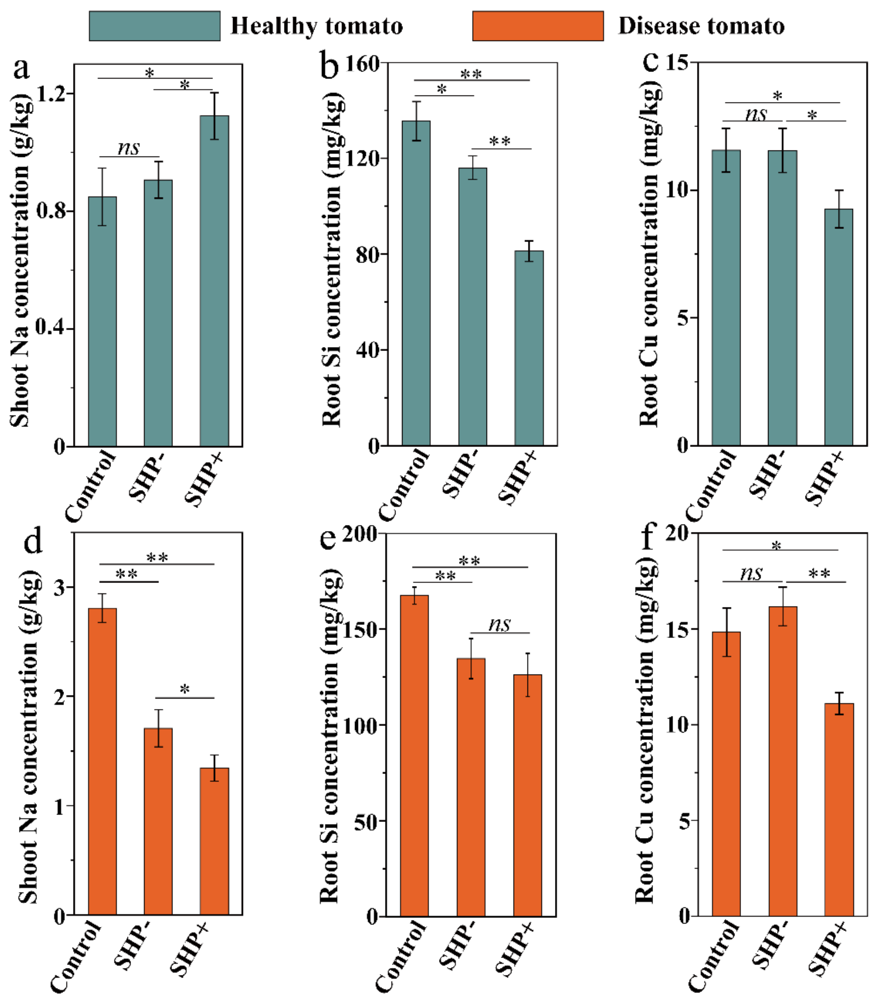

Figure 6. Concentrations of (a) Healthy shoot Na, (b) Healthy root Si, (c) Healthy root Cu, (d) Disease shoot Na, (e) Disease root Si, and (f) Disease root Cu in the greenhouse tomato plants, as determined by ICP-OES. The error bars represent the standard error. A one-way ANOVA with Tukey's multiple comparisons post hoc test was used to evaluate statistical significance. *$p < 0.05$, **$p < 0.01$.

4. Conclusion

This study demonstrates the significant role of nanoscale iron oxide in modulating disease resistance and nutrient accumulation in tomato plants through a foliar application. The effect of nanoparticle surface charge was determined both experimentally and computationally. Although both SHP+ and SHP-nanoparticles significantly suppressed Fusarium disease, SHP+ was more effective; SHP+ increased Fe content in shoots by 136.5% under healthy conditions and 175.3% under diseased conditions, compared to SHP-, which increased Fe by 103.8% and 164.8%, respectively. SHP+ also enhanced Si content by 24% and 32.5% and mitigated excessive Cu and Na accumulation due to the disease more effectively than SHP-. In addition, a superior effect of nanoscale versus bulk iron oxide was evident; nanoscale forms exerted significantly greater disease suppression and were not phytotoxic. Theoretical calculations through computational modeling align with these charge dependent experimental results, underscoring the critical influence of NP surface charge on nutrient dynamics and plant health. Further mechanistic investigations at molecular level are needed to understand more complex interactions between SHP+ and plants, as well as the potential effect of PEI on disease suppression. These findings highlight the potential application and optimization of charged Fe_3O_4 NPs as plant protection to enhance disease resistance for better crop productivity.

Supporting Information

Experimental and Result sections; DLS data for SHP- and SHP+; comparison of Coulomb and softened Slater potentials and forces; composition of simulated lipids and proportions of each component; concentrations of shoot Na, root Si, and root Cu in the greenhouse tomato plants.

Acknowledgments

This work was supported by the NSF Center for Sustainable Nanotechnology under grant number CHE-2001611; The NSF CSN is part of the Center for Chemical Innovation Program.

Author Statement

Chaoyi Deng: Conceptualization, Investigation, Methodology, Writing- Original draft, Reviewing and editing **Yinhan Wang:** Software, Methodology, Writing- Original draft, Reviewing and editing **Christopher Castillo:** Investigation, Writing- Original draft **Yinong Zhao:** Methodology, Validation

Wandi Xu: Writing - Original Draft **Jiapan Lian:** Software, Visualization **Kevin Rodriguez-Otero:** Investigation **Hannah J. Brown:** Investigation **Keni Cota-Ruiz:** Writing - Review and Editing **Wade H. Elmer:** Resources **Christian O. Dimkpa:** Resources, Writing - Review and Editing **Juan Pablo Giraldo:** Resources, Supervision, Review and Editing **Yi Wang:** Conceptualization, Investigation, Writing- Original draft, Reviewing and editing, Supervision **Rigoberto Hernandez:** Resources, Supervision, Writing - Review and Editing, Funding acquisition **Jason C. White:** Conceptualization, Investigation, Reviewing and editing, Supervision, Resources, Funding acquisition

(1) van Dijk, M.; Morley, T.; Rau, M. L.; Saghai, Y. A Meta-Analysis of Projected Global Food Demand and Population at Risk of Hunger for the Period 2010–2050. *Nature Food 2021 2:7* **2021**, *2* (7), 494–501. https://doi.org/10.1038/s43016-021-00322-9.

(2) Urso, J. H.; Gilbertson, L. M. Atom Conversion Efficiency: A New Sustainability Metric Applied to Nitrogen and Phosphorus Use in Agriculture. *ACS Sustain Chem Eng* **2018**, *6* (4), 4453–4463. https://doi.org/10.1021/ACSSUSCHEMENG.7B03600/ASSET/IMAGES/LARGE/SC-2017-03600Q_0002.JPEG.

(3) Shahzad, A.; Ullah, S.; Dar, A. A.; Sardar, M. F.; Mehmood, T.; Tufail, M. A.; Shakoor, A.; Haris, M. Nexus on Climate Change: Agriculture and Possible Solution to Cope Future Climate Change Stresses. *Environmental Science and Pollution Research* **2021**, *28* (12), 14211–14232. https://doi.org/10.1007/S11356-021-12649-8/METRICS.

(4) Vaidya, S.; Deng, C.; Wang, Y.; Zuverza-Mena, N.; Dimkpa, C.; White, J. C. Nanotechnology in Agriculture: A Solution to Global Food Insecurity in a Changing Climate? *NanoImpact* **2024**, *34*, 100502. https://doi.org/10.1016/J.IMPACT.2024.100502.

(5) Savary, S.; Willocquet, L.; Pethybridge, S. J.; Esker, P.; McRoberts, N.; Nelson, A. The Global Burden of Pathogens and Pests on Major Food Crops. *Nature Ecology & Evolution 2019 3:3* **2019**, *3* (3), 430–439. https://doi.org/10.1038/s41559-018-0793-y.

(6) Gordon, T. R. Fusarium Oxysporum and the Fusarium Wilt Syndrome. *https://doi.org/10.1146/annurev-phyto-080615-095919* **2017**, *55*, 23–39. https://doi.org/10.1146/ANNUREV-PHYTO-080615-095919.

(7) Dean, R.; Van Kan, J. A. L.; Pretorius, Z. A.; Hammond-Kosack, K. E.; Di Pietro, A.; Spanu, P. D.; Rudd, J. J.; Dickman, M.; Kahmann, R.; Ellis, J.; Foster, G. D. The Top 10 Fungal Pathogens in Molecular Plant Pathology. *Mol Plant Pathol* **2012**, *13* (4), 414–430. https://doi.org/10.1111/J.1364-3703.2011.00783.X.

(8) Haydar, M. S.; Ghosh, D.; Roy, S. Slow and Controlled Release Nanofertilizers as an Efficient Tool for Sustainable Agriculture: Recent Understanding and Concerns. *Plant Nano Biology* **2024**, *7*, 100058. https://doi.org/10.1016/J.PLANA.2024.100058.

(9) Usman, M.; Farooq, M.; Wakeel, A.; Nawaz, A.; Cheema, S. A.; Rehman, H. ur; Ashraf, I.; Sanaullah, M. Nanotechnology in Agriculture: Current Status, Challenges and Future Opportunities. *Science of The Total Environment* **2020**, *721*, 137778. https://doi.org/10.1016/J.SCITOTENV.2020.137778.

(10) Jomeyazdian, A.; Pirnia, M.; Alaei, H.; Taheri, A.; Sarani, S. Control of Fusarium Wilt Disease of Tomato and Improvement of Some Growth Factors through Green Synthesized Zinc Oxide Nanoparticles. *Eur J Plant Pathol* **2024**, 1–13. https://doi.org/10.1007/S10658-024-02831-2/FIGURES/8.

(11) Elmer, W. H.; White, J. C. The Use of Metallic Oxide Nanoparticles to Enhance Growth of Tomatoes and Eggplants in Disease Infested Soil or Soilless Medium. *Environ Sci Nano* **2016**, *3* (5), 1072–1079. https://doi.org/10.1039/C6EN00146G.

(12) Wang, Y.; Deng, C.; Shen, Y.; Borgatta, J.; Dimkpa, C. O.; Xing, B.; Dhankher, O. P.; Wang, Z.; White, J. C.; Elmer, W. H. Surface Coated Sulfur Nanoparticles Suppress Fusarium Disease in Field Grown Tomato: Increased Yield and Nutrient Biofortification. *J Agric Food Chem* **2022**, *70* (45), 14377–14385. https://doi.org/10.1021/ACS.JAFC.2C05255/SUPPL_FILE/JF2C05255_SI_001.PDF.

(13) Lopez-Lima, D.; Mtz-Enriquez, A. I.; Carrión, G.; Basurto-Cereceda, S.; Pariona, N. The Bifunctional Role of Copper Nanoparticles in Tomato: Effective Treatment for Fusarium Wilt and Plant Growth Promoter. *Sci Hortic* **2021**, *277*, 109810. https://doi.org/10.1016/J.SCIENTA.2020.109810.

(14) Mendez, O. E.; Astete, C. E.; Cueto, R.; Eitzer, B.; Hanna, E. A.; Salinas, F.; Tamez, C.; Wang, Y.; White, J. C.; Sabliov, C. M. Lignin Nanoparticles as Delivery Systems to Facilitate Translocation of Methoxyfenozide in Soybean (Glycine Max). *J Agric Food Res* **2022**, *7*, 100259. https://doi.org/10.1016/J.JAFR.2021.100259.

(15) Deng, C.; Protter, C. R.; Wang, Y.; Borgatta, J.; Zhou, J.; Wang, P.; Goyal, V.; Brown, H. J.; Rodriguez-Otero, K.; Dimkpa, C. O.; Hernandez, R.; Hamers, R. J.; White, J. C.; Elmer, W. H. Nanoscale CuO Charge and Morphology Control Fusarium Suppression and Nutrient Biofortification in Field-Grown Tomato and Watermelon. *Science of The Total Environment* **2023**, *905*, 167799. https://doi.org/10.1016/J.SCITOTENV.2023.167799.

(16) Tuga, B.; O'Keefe, T.; Deng, C.; Ligocki, A. T.; White, J. C.; Haynes, C. L. Designing Nanoparticles for Sustainable Agricultural Applications. *Trends Chem* **2023**, *5* (11), 814–826. https://doi.org/10.1016/j.trechm.2023.07.004.

(17) Borgatta, J.; Ma, C.; Hudson-Smith, N.; Elmer, W.; Plaza Pérez, C. D.; De La Torre-Roche, R.; Zuverza-Mena, N.; Haynes, C. L.; White, J. C.; Hamers, R. J. Copper Based Nanomaterials Suppress Root Fungal Disease in Watermelon (Citrullus Lanatus): Role of Particle Morphology, Composition and Dissolution Behavior. *ACS Sustain Chem Eng* **2018**, *6* (11), 14847–14856. https://doi.org/10.1021/ACSSUSCHEMENG.8B03379/SUPPL_FILE/SC8B03379_SI_001.PDF.

(18) Ma, C.; Borgatta, J.; Hudson, B. G.; Tamijani, A. A.; De La Torre-Roche, R.; Zuverza-Mena, N.; Shen, Y.; Elmer, W.; Xing, B.; Mason, S. E.; Hamers, R. J.; White, J. C. Advanced Material Modulation of Nutritional and Phytohormone Status Alleviates Damage from Soybean Sudden Death Syndrome. *Nature Nanotechnology 2020 15:12* **2020**, *15* (12), 1033–1042. https://doi.org/10.1038/s41565-020-00776-1.

(19) Zhu, H.; Han, J.; Xiao, J. Q.; Jin, Y. Uptake, Translocation, and Accumulation of Manufactured Iron Oxide Nanoparticles by Pumpkin Plants. *Journal of Environmental Monitoring* **2008**, *10* (6), 713–717. https://doi.org/10.1039/B805998E.

(20) El-Batal, A. I.; El-Sayyad, G. S.; Al-shammari, B. M.; Abdelaziz, A. M.; Nofel, M. M.; Gobara, M.; Elkhatib, W. F.; Eid, N. A.; Salem, M. S.; Attia, M. S. Protective Role of Iron Oxide Nanocomposites on Disease Index, and Biochemical Resistance Indicators against Fusarium Oxysporum Induced-Cucumber Wilt Disease: In Vitro, and in Vivo Studies. *Microb Pathog* **2023**, *180*, 106131. https://doi.org/10.1016/J.MICPATH.2023.106131.

(21) Feng, Y.; Kreslavski, V. D.; Shmarev, A. N.; Ivanov, A. A.; Zharmukhamedov, S. K.; Kosobryukhov, A.; Yu, M.; Allakhverdiev, S. I.; Shabala, S. Effects of Iron Oxide Nanoparticles (Fe3O4) on Growth,

Photosynthesis, Antioxidant Activity and Distribution of Mineral Elements in Wheat (Triticum Aestivum) Plants. *Plants* **2022**, *11* (14), 1894. https://doi.org/10.3390/PLANTS11141894/S1.

(22) Wang, Y.; Wang, S.; Xu, M.; Xiao, L.; Dai, Z.; Li, J. The Impacts of γ-Fe2O3 and Fe3O4 Nanoparticles on the Physiology and Fruit Quality of Muskmelon (Cucumis Melo) Plants. *Environmental Pollution* **2019**, *249*, 1011–1018. https://doi.org/10.1016/J.ENVPOL.2019.03.119.

(23) Kim, K.; Jeon, S. J.; Hu, P.; Anastasia, C. M.; Beimers, W. F.; Giraldo, J. P.; Pedersen, J. A. Sulfolipid Density Dictates the Extent of Carbon Nanodot Interaction with Chloroplast Membranes. *Environ Sci Nano* **2022**, *9* (8), 2691–2703. https://doi.org/10.1039/D2EN00158F.

(24) Gao, X.; Lowry, G. V. Progress towards Standardized and Validated Characterizations for Measuring Physicochemical Properties of Manufactured Nanomaterials Relevant to Nano Health and Safety Risks. *NanoImpact* **2018**, *9*, 14–30. https://doi.org/10.1016/J.IMPACT.2017.09.002.

(25) *General handling and storage of organic soluble iron oxide ...* https://www.yumpu.com/en/document/read/39902670/general-handling-and-storage-of-organic-soluble-iron-oxide- (accessed 2024-01-02).

(26) Yan, L.; Li, P.; Zhao, X.; Ji, R.; Zhao, L. Physiological and Metabolic Responses of Maize (Zea Mays) Plants to Fe3O4 Nanoparticles. *Science of The Total Environment* **2020**, *718*, 137400. https://doi.org/10.1016/J.SCITOTENV.2020.137400.

(27) Wang, Y.; Chen, S.; Deng, C.; Shi, X.; Cota-Ruiz, K.; White, J. C.; Zhao, L.; Gardea-Torresdey, J. L. Metabolomic Analysis Reveals Dose-Dependent Alteration of Maize (Zea Mays L.) Metabolites and Mineral Nutrient Profiles upon Exposure to Zerovalent Iron Nanoparticles. *NanoImpact* **2021**, *23*, 100336. https://doi.org/10.1016/J.IMPACT.2021.100336.

(28) Borgatta, J.; Shen, Y.; Tamez, C.; Green, C.; Orbeck, J. K. H.; Cahill, M. S.; Protter, C.; Deng, C.; Wang, Y.; Elmer, W.; White, J. C.; Hamers, R. J. Influence of CuO Nanoparticle Aspect Ratio and Surface Charge on Disease Suppression in Tomato (Solanum Lycopersicum). *J Agric Food Chem* **2023**. https://doi.org/10.1021/ACS.JAFC.2C09153.

(29) Wang, Y.; Deng, C.; Elmer, W. H.; Dimkpa, C. O.; Sharma, S.; Navarro, G.; Wang, Z.; Lareau, J.; Steven, B. T.; Wang, Z.; Zhao, L.; Li, C.; Dhankher, O. P.; Gardea-Torresdey, J. L.; Xing, B.; White, J. C. Therapeutic Delivery of Nanoscale Sulfur to Suppress Disease in Tomatoes: In Vitro Imaging and Orthogonal Mechanistic Investigation. *ACS Nano* **2022**, *16* (7), 11204–11217. https://doi.org/10.1021/ACSNANO.2C04073/SUPPL_FILE/NN2C04073_SI_008.AVI.

(30) Jeger, M. J.; Viljanen-Rollinson, S. L. H. The Use of the Area under the Disease-Progress Curve (AUDPC) to Assess Quantitative Disease Resistance in Crop Cultivars. *Theoretical and Applied Genetics* **2001**, *102* (1), 32–40. https://doi.org/10.1007/S001220051615/METRICS.

(31) Thompson, A. P.; Aktulga, H. M.; Berger, R.; Bolintineanu, D. S.; Brown, W. M.; Crozier, P. S.; in 't Veld, P. J.; Kohlmeyer, A.; Moore, S. G.; Nguyen, T. D.; Shan, R.; Stevens, M. J.; Tranchida, J.; Trott, C.; Plimpton, S. J. LAMMPS - a Flexible Simulation Tool for Particle-Based Materials Modeling at the Atomic, Meso, and Continuum Scales. *Comput Phys Commun* **2022**, *271*. https://doi.org/10.1016/J.CPC.2021.108171.

(32) Groot, R. D.; Warren, P. B. Dissipative Particle Dynamics: Bridging the Gap between Atomistic and Mesoscopic Simulation. *J Chem Phys* **1997**, *107* (11), 4423–4435. https://doi.org/10.1063/1.474784.

(33) Wang, Y.; Hernandez, R. Construction of Multiscale Dissipative Particle Dynamics (DPD) Models from Other Coarse-Grained Models. *ACS Omega* **2024**. https://doi.org/10.1021/ACSOMEGA.4C01868/ASSET/IMAGES/LARGE/AO4C01868_0009.JPEG.

(34) González-Melchor, M.; Mayoral, E.; Velázquez, M. E.; Alejandre, J. Electrostatic Interactions in Dissipative Particle Dynamics Using the Ewald Sums. *Journal of Chemical Physics* **2006**, *125* (22). https://doi.org/10.1063/1.2400223/953750.

(35) Monticelli, L.; Kandasamy, S. K.; Periole, X.; Larson, R. G.; Tieleman, D. P.; Marrink, S. J. The MARTINI Coarse-Grained Force Field: Extension to Proteins. *J Chem Theory Comput* **2008**, *4* (5), 819–834. https://doi.org/10.1021/CT700324X.

(36) Popko, J. Lipid Composition of Arabidopsis Thaliana Leaves. *Encyclopedia of Lipidomics* **2017**, 1–11. https://doi.org/10.1007/978-94-007-7864-1_120-1.

(37) Qi, Y.; Ingólfsson, H. I.; Cheng, X.; Lee, J.; Marrink, S. J.; Im, W. CHARMM-GUI Martini Maker for Coarse-Grained Simulations with the Martini Force Field. *J Chem Theory Comput* **2015**, *11* (9), 4486–4494. https://doi.org/10.1021/ACS.JCTC.5B00513/SUPPL_FILE/CT5B00513_SI_001.PDF.

(38) Jo, S.; Kim, T.; Iyer, V. G.; Im, W. CHARMM-GUI: A Web-Based Graphical User Interface for CHARMM. *J Comput Chem* **2008**, *29* (11), 1859–1865. https://doi.org/10.1002/JCC.20945.

(39) Hsu, P. C.; Bruininks, B. M. H.; Jefferies, D.; Cesar Telles de Souza, P.; Lee, J.; Patel, D. S.; Marrink, S. J.; Qi, Y.; Khalid, S.; Im, W. CHARMM-GUI Martini Maker for Modeling and Simulation of Complex Bacterial Membranes with Lipopolysaccharides. *J Comput Chem* **2017**, *38* (27), 2354–2363. https://doi.org/10.1002/JCC.24895.

(40) Litunov, S. N.; Gusak, E. N.; Toshhakova, Y. D.; Li, S.; Gao, L.; Liu, H.; Jannah, N. R.; Onggo, D. Synthesis of Fe3O4 Nanoparticles for Colour Removal of Printing Ink Solution. *J Phys Conf Ser* **2019**, *1245* (1), 012040. https://doi.org/10.1088/1742-6596/1245/1/012040.

(41) *IR Spectrum Table*. https://www.sigmaaldrich.com/US/en/technical-documents/technical-article/analytical-chemistry/photometry-and-reflectometry/ir-spectrum-table (accessed 2024-01-10).

(42) Zia-ur-Rehman, M.; Mfarrej, M. F. B.; Usman, M.; Anayatullah, S.; Rizwan, M.; Alharby, H. F.; Abu Zeid, I. M.; Alabdallah, N. M.; Ali, S. Effect of Iron Nanoparticles and Conventional Sources of Fe on Growth, Physiology and Nutrient Accumulation in Wheat Plants Grown on Normal and Salt-Affected Soils. *J Hazard Mater* **2023**, *458*, 131861. https://doi.org/10.1016/J.JHAZMAT.2023.131861.

(43) Li, M.; Zhang, P.; Adeel, M.; Guo, Z.; Chetwynd, A. J.; Ma, C.; Bai, T.; Hao, Y.; Rui, Y. Physiological Impacts of Zero Valent Iron, Fe3O4 and Fe2O3 Nanoparticles in Rice Plants and Their Potential as Fe Fertilizers. *Environmental Pollution* **2021**, *269*, 116134. https://doi.org/10.1016/J.ENVPOL.2020.116134.

(44) Elbasuney, S.; El-Sayyad, G. S.; Attia, M. S.; Abdelaziz, A. M. Ferric Oxide Colloid: Towards Green Nano-Fertilizer for Tomato Plant with Enhanced Vegetative Growth and Immune Response Against Fusarium Wilt Disease. *J Inorg Organomet Polym Mater* **2022**, *32* (11), 4270–4283. https://doi.org/10.1007/S10904-022-02442-6/FIGURES/12.

(45) Bidabadi, S. S.; Sabbatini, P.; VanderWeide, J. Iron Oxide (Fe2O3) Nanoparticles Alleviate PEG-Simulated Drought Stress in Grape (Vitis Vinifera L.) Plants by Regulating Leaf Antioxidants. *Sci Hortic* **2023**, *312*, 111847. https://doi.org/10.1016/J.SCIENTA.2023.111847.

(46) Sameer, A.; Rabia, S.; Amanat, A.; Khan, A.; Hussain, A.; Ali, B.; Zaheer, M. S.; Ali, H.; Fareed, K.; Sheteiwy, M. S.; Ali, S. Combined Application of Zinc Oxide and Iron Nanoparticles Enhanced Red Sails Lettuce Growth and Antioxidants Enzymes Activities While Reducing the Chromium Uptake by Plants Grown in a Cr-Contaminated Soil. **2023**. https://doi.org/10.21203/RS.3.RS-2346445/V1.

(47) Lau, E. C. H. T.; Carvalho, L. B.; Pereira, A. E. S.; Montanha, G. S.; Corrêa, C. G.; Carvalho, H. W. P.; Ganin, A. Y.; Fraceto, L. F.; Yiu, H. H. P. Localization of Coated Iron Oxide (Fe3O4) Nanoparticles on Tomato Seeds and Their Effects on Growth. *ACS Appl Bio Mater* **2020**, *3* (7), 4109–4117. https://doi.org/10.1021/ACSABM.0C00216/ASSET/IMAGES/LARGE/MT0C00216_0007.JPEG.

(48) Iannone, M. F.; Groppa, M. D.; Zawoznik, M. S.; Coral, D. F.; Fernández van Raap, M. B.; Benavides, M. P. Magnetite Nanoparticles Coated with Citric Acid Are Not Phytotoxic and Stimulate Soybean and Alfalfa Growth. *Ecotoxicol Environ Saf* **2021**, *211*, 111942. https://doi.org/10.1016/J.ECOENV.2021.111942.

(49) Briat, J. F.; Curie, C.; Gaymard, F. Iron Utilization and Metabolism in Plants. *Curr Opin Plant Biol* **2007**, *10* (3), 276–282. https://doi.org/10.1016/J.PBI.2007.04.003.

(50) Rout, G. R.; Sahoo, S. ROLE OF IRON IN PLANT GROWTH AND METABOLISM. *Reviews in Agricultural Science* **2015**, *3* (0), 1–24. https://doi.org/10.7831/RAS.3.1.

(51) Silva, S.; Dias, M. C.; Pinto, D. C. G. A.; Silva, A. M. S. Metabolomics as a Tool to Understand Nano-Plant Interactions: The Case Study of Metal-Based Nanoparticles. *Plants 2023, Vol. 12, Page 491* **2023**, *12* (3), 491. https://doi.org/10.3390/PLANTS12030491.

(52) Hu, J.; Xianyu, Y. When Nano Meets Plants: A Review on the Interplay between Nanoparticles and Plants. *Nano Today* **2021**, *38*, 101143. https://doi.org/10.1016/J.NANTOD.2021.101143.

(53) Dimkpa, C. *Endocytobiosis and Cell Research Microbial Siderophores: Production, Detection and Application in Agriculture and Environment*; 2016; Vol. 27.

(54) Sharma, S.; Pandey, R.; Dimkpa, C. O.; Kumar, A.; Bindraban, P. S. Growth Stage-Dependent Foliar Application of Iron Improves Its Mobilisation Towards Grain and Enhances Fe Use Efficiency in Rice. *J Plant Growth Regul* **2023**, *42* (9), 5628–5641. https://doi.org/10.1007/S00344-023-10944-X/METRICS.

(55) Wu, M.; Vartanian, A. M.; Chong, G.; Pandiakumar, A. K.; Hamers, R. J.; Hernandez, R.; Murphy, C. J. Solution NMR Analysis of Ligand Environment in Quaternary Ammonium-Terminated Self-Assembled Monolayers on Gold Nanoparticles: The Effect of Surface Curvature and Ligand

Structure. *J Am Chem Soc* **2019**, *141* (10), 4316–4327. https://doi.org/10.1021/JACS.8B11445/ASSET/IMAGES/LARGE/JA-2018-11445J_0016.JPEG.

(56) Mahajan, S.; Tang, T. Martini Coarse-Grained Model for Polyethylenimine. *J Comput Chem* **2019**, *40* (3), 607–618. https://doi.org/10.1002/JCC.25747.

(57) Chen, J.; Liu, S.; Hou, Y.; Luo, Y.; Han, W. Determination of Leaf PH without Grinding the Sample: Is It Closer to the Reality? *Forests 2022, Vol. 13, Page 1640* **2022**, *13* (10), 1640. https://doi.org/10.3390/F13101640.

(58) Subbarao, G. V.; Ito, O.; Berry, W. L.; Wheeler, R. M. Sodium—A Functional Plant Nutrient. *CRC Crit Rev Plant Sci* **2003**, *22* (5), 391–416. https://doi.org/10.1080/07352680390243495.

(59) Kang, H.; Elmer, W.; Shen, Y.; Zuverza-Mena, N.; Ma, C.; Botella, P.; White, J. C.; Haynes, C. L. Silica Nanoparticle Dissolution Rate Controls the Suppression of Fusarium Wilt of Watermelon (Citrullus Lanatus). *Environ Sci Technol* **2021**, *55* (20), 13513–13522. https://doi.org/10.1021/ACS.EST.0C07126/ASSET/IMAGES/LARGE/ES0C07126_0004.JPEG.

(60) Mahawar, L.; Ramasamy, K. P.; Suhel, M.; Prasad, S. M.; Živčák, M.; Brestic, M.; Rastogi, A.; Skalický, M. Silicon Nanoparticles: Comprehensive Review on Biogenic Synthesis and Applications in Agriculture. *Environ Res* **2023**, *232*, 116292. https://doi.org/10.1016/J.ENVRES.2023.116292.